Neuropilin-1 is a host factor for SARS-CoV-2 infection

CORONAVIRUS

Neuropilin-1 is a host factor for SARS-CoV-2 infection

James L. Daly[1]*, Boris Simonetti[1]*†, Katja Klein[2]*, Kai-En Chen[3]‡, Maia Kavanagh Williamson[2]‡, Carlos Antón-Plágaro[1]‡, Deborah K. Shoemark[4], Lorena Simón-Gracia[5], Michael Bauer[6], Reka Hollandi[7], Urs F. Greber[6], Peter Horvath[7,8], Richard B. Sessions[1], Ari Helenius[9], Julian A. Hiscox[10,11], Tambet Teesalu[5], David A. Matthews[2], Andrew D. Davidson[2], Brett M. Collins[3], Peter J. Cullen[1]†, Yohei Yamauchi[2,12]†

Severe acute respiratory syndrome coronavirus 2 (SARS-CoV-2), the causative agent of coronavirus disease 2019 (COVID-19), uses the viral spike (S) protein for host cell attachment and entry. The host protease furin cleaves the full-length precursor S glycoprotein into two associated polypeptides: S1 and S2. Cleavage of S generates a polybasic Arg-Arg-Ala-Arg carboxyl-terminal sequence on S1, which conforms to a C-end rule (CendR) motif that binds to cell surface neuropilin-1 (NRP1) and NRP2 receptors. We used x-ray crystallography and biochemical approaches to show that the S1 CendR motif directly bound NRP1. Blocking this interaction by RNA interference or selective inhibitors reduced SARS-CoV-2 entry and infectivity in cell culture. NRP1 thus serves as a host factor for SARS-CoV-2 infection and may potentially provide a therapeutic target for COVID-19.

Severe acute respiratory syndrome coronavirus 2 (SARS-CoV-2) is the coronavirus responsible for the current coronavirus disease 2019 (COVID-19) pandemic (*1*, *2*). A marked difference between the spike (S) protein of SARS-CoV-2 and SARS-CoV is the presence, in the former, of a polybasic sequence motif, Arg-Arg-Ala-Arg (RRAR), at the S1/S2 boundary. It provides a cleavage site for a host proprotein convertase, furin (*3*–*5*) (fig. S1A). The resulting two proteins, S1 and S2, remain noncovalently associated, with the serine protease TMPRSS2 further priming S2 (*6*). Furin-mediated processing increases infectivity and affects the tropism of SARS-CoV-2, whereas furin inhibition diminishes SARS-CoV-2 entry, and deletion of the polybasic site in the S protein reduces syncytia formation in cell culture (*3*–*5*, *7*).

The C terminus of the S1 protein generated by furin cleavage has an amino acid sequence (^{682}RRAR^{685}) that conforms to a [R/K]XX[R/K] motif, termed the "C-end rule" (CendR) (fig. S1B) (*8*). CendR peptides bind to neuropilin-1 (NRP1) and NRP2, transmembrane receptors that regulate pleiotropic biological processes, including axon guidance, angiogenesis, and vascular permeability (*8*–*10*). To explore the possibility that the SARS-CoV-2 S1 protein may associate with neuropilins, we generated a green fluorescent protein (GFP)–tagged S1 construct (GFP-S1) (fig. S1C). When expressed in human embryonic kidney 293T (HEK293T) cells engineered to express the SARS-CoV-2 receptor angiotensin-converting enzyme 2 (ACE2), GFP-S1 immunoprecipitated endogenous NRP1 and ACE2 (Fig. 1A). We transiently coexpressed NRP1-mCherry and either GFP-S1 or GFP-S1 ΔRRAR (a deletion of the terminal ^{682}RRAR^{685} residues) in HEK293T cells. NRP1 immunoprecipitated the S1 protein, and deletion of the CendR motif reduced this association (Fig. 1B). Comparable binding was also observed with mCherry-NRP2, a receptor with high homology to NRP1 (fig. S1, D and E). In both cases, residual binding was observed with the ΔRRAR mutant, indicating an additional CendR-independent association between neuropilins and the S1 protein.

To probe the functional relevance of this interaction, we generated HeLa wild-type and NRP1 knockout (KO) cell lines stably expressing ACE2, designated as HeLa^{wt}+ACE2 and HeLa^{NRP1KO}+ACE2, respectively (the level of ACE2 expression was comparable between these lines) (fig. S1F). Using a clinical isolate SARS-CoV-2 (SARS-CoV-2/human/Liverpool/REMRQ001/2020), we performed viral infection assays and fixed the cells at 6 and 16 hours postinfection (hpi). SARS-CoV-2 infection was reduced in HeLa^{NRP1KO}+ACE2 relative to HeLa^{wt}+ACE2 (Fig. 1C). HeLa cells lacking ACE2 expression were not infected (fig. S1G). In Caco-2 cells, a human colon adenocarcinoma cell line endogenously expressing ACE2 and widely used in COVID-19 studies, the suppression of NRP1 expression by short hairpin RNA (shRNA) greatly reduced SARS-CoV-2 infection at both 7 and 16 hpi, respectively, whereas that of vesicular stomatitis virus (VSV) pseudotyped with VSV-G was unaffected (Fig. 1D and figs. S1H and S2A). To determine if NRP1 was required for early virus infection, we established a sequential staining procedure using antibodies against SARS-CoV-2 S and N proteins to distinguish extracellular and intracellular viral particles (fig. S2B). Although NRP1 depletion did not affect SARS-CoV-2 binding to the Caco-2 cell surface (Fig. 1E), virus uptake was halved in NRP1-depleted cells compared to control cells after 30 min of internalization (Fig. 1F). Thus, NRP1 enhances SARS-CoV-2 entry and infection.

We also observed that SARS-CoV-2–infected HeLa^{wt}+ACE2 cells displayed a multinucleated syncytia cell pattern, as reported by others (Fig. 1C) (*5*). Using an image analysis algorithm and supervised machine learning (fig. S2, C to F) (*11*), we quantified syncytia of infected HeLa^{wt}+ACE2 and HeLa^{NRP1KO}+ACE2 cells. At 16 hpi, the majority of HeLa^{wt}+ACE2 cells formed syncytia, whereas in HeLa^{NRP1KO}+ACE2 cells, this phenotype was reduced (fig. S2G). When infected with a SARS-CoV-2 isolate lacking the furin cleavage site (SARS-CoV-2 ΔS1/S2) (fig. S1A), the differences in infection and syncytia formation were less pronounced (fig. S2, H and I). However, a significant decrease in infection of HeLa^{NRP1KO}+ACE2 was still observed at 16 hpi, indicating that NRP1 may additionally influence infection through a CendR-independent mechanism (fig. S2H).

The extracellular regions of NRP1 and NRP2 are composed of two CUB domains (a1 and a2), two coagulation factor domains (b1 and b2), and a MAM domain (*9*). Of these, the b1 domain contains the specific binding site for CendR peptides (fig. S3A) (*12*). Accordingly, the mCherry-b1 domain of NRP1 immunoprecipitated GFP-S1, and a shortened GFP-S1 construct spanning residues 493 to 685 (figs. S1C and S3B). Isothermal titration calorimetry (ITC) established that the b1 domain of NRP1 directly bound a synthetic S1 CendR peptide (^{679}NSPRRAR^{685}) with an affinity of 20.3 μM at pH 7.5, which was enhanced to 13.0 μM at pH 5.5 (Fig. 2A). Binding was not observed to an S1 CendR peptide in which the C-terminal arginine was mutated to alanine (^{679}NSPRRAA^{685}) (Fig. 2A). We cocrystallized the NRP1 b1 domain in complex with the S1 CendR peptide (Fig. 2B). The resolved 2.35-Å structure revealed four molecules of b1 with electron density of the S1 CendR peptide clearly visible in the asymmetric unit (fig. S3C). S1 CendR peptide binding displayed strong similarity to the previously solved structure of NRP1 b1 domain in complex with

[1]School of Biochemistry, Faculty of Life Sciences, Biomedical Sciences Building, University of Bristol, Bristol BS8 1TD, UK. [2]School of Cellular and Molecular Medicine, Faculty of Life Sciences, Biomedical Sciences Building, University of Bristol, Bristol BS8 1TD, UK. [3]Institute for Molecular Bioscience, the University of Queensland, St. Lucia, QLD 4072, Australia. [4]School of Biochemistry and BrisSynBio Centre, Faculty of Life Sciences, Biomedical Sciences Building, University of Bristol, Bristol BS8 1TD, UK. [5]Laboratory of Cancer Biology, Institute of Biomedicine and Translational Medicine, University of Tartu, Tartu, Estonia. [6]Department of Molecular Life Sciences, University of Zurich, Winterthurerstrasse 190, 8057 Zürich, Switzerland. [7]Synthetic and Systems Biology Unit, Biological Research Centre (BRC), Szeged, Hungary. [8]Institute for Molecular Medicine Finland, University of Helsinki, Helsinki, Finland. [9]Institute of Biochemistry, ETH Zurich, Zurich, Switzerland. [10]Institute of Infection, Veterinary and Ecological Sciences, University of Liverpool, Liverpool, UK. [11]Singapore Immunology Network, Agency for Science, Technology, and Research, 138648, Singapore. [12]Division of Biological Science, Graduate School of Science, Nagoya University, Furo-cho, Chikusa-ku, Nagoya, 464-8601, Japan.
*These authors contributed equally to this work.
†Corresponding author. Email: bs13866@bristol.ac.uk (B.S.); pete.cullen@bristol.ac.uk (P.J.C.); yohei.yamauchi@bristol.ac.uk (Y.Y.)
‡These authors contributed equally to this work.

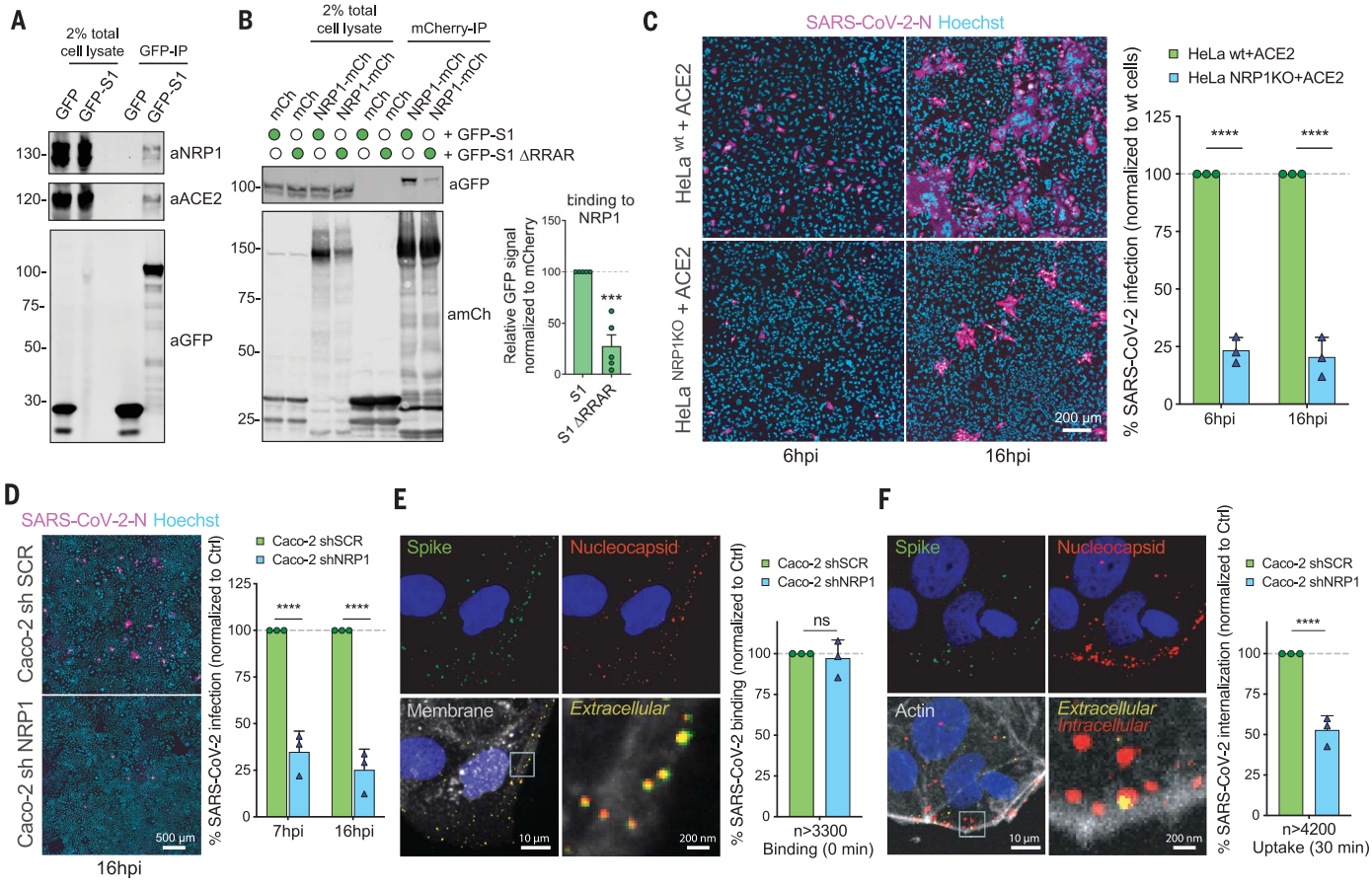

Fig. 1. NRP1 Interacts with S1 and enhances SARS-CoV-2 infection. (**A**) HEK293T cells transduced to express ACE2 were transfected to express GFP or GFP-tagged S1 and lysed after 24 hours. The lysates were subjected to GFP-nanotrap, and the immune isolates were blotted for ACE2 and NRP1 (N = 3 independent experiments). (**B**) HEK293T cells were cotransfected to express GFP-tagged S1 or GFP-S1 ΔRRAR and mCherry or mCherry-tagged NRP1 and subjected to GFP-nanotrap (N = 5 independent experiments). Two-tailed unpaired t test; P = 0.0002. (**C**) HeLa^{wt}+ACE2 and HeLa$^{NRP1\ KO}$+ACE2 cells were infected with SARS-CoV-2. Cells were fixed at 6 or 16 hpi and stained for N protein (magenta) and Hoechst (cyan), and virus infectivity was quantified (N = 3 independent experiments). Two-tailed unpaired t test; P = 0.00002 and 0.00088. Scale bar, 200 µm. (**D**) Caco-2 cells expressing shRNA against NRP1 or a nontargeting control (SCR) were infected with SARS-CoV-2 and fixed at 7 or 16 hpi. The cells were stained for N protein (magenta) and Hoechst (cyan), and infectivity was quantified (N = 3 independent experiments). Two-tailed unpaired t test; P = 0.0005 and 0.00032. Scale bar, 500 µm. (**E**) Caco-2 shSCR or shNRP1 cells were inoculated with a multiplicity of infection (MOI) = 50 of SARS-CoV-2 and incubated in the cold for 60 min, and fixed. A two-step antibody staining procedure was performed with antibodies against S and N to distinguish external (green) and total (red) virus particles, and the binding of particles per cell was quantified for >3300 particles per condition (N = 3 independent experiments). Two-tailed unpaired t test; P = 0.6859. (**F**) Caco-2 shSCR or shNRP1 cells were bound with SARS-CoV-2 as in (E), followed by incubation at 37°C for 30 min. The cells were fixed and stained as in (E). Viral uptake was quantified for >4200 particles per condition (N = 3 independent experiments). Two-tailed unpaired t test; P = 0.00079. Scale bars [(E) and (F)], 10 µm and 200 nm (magnified panels). The square regions were enlarged. The bars, error bars, and circles and triangles represent the mean, SEM (B) and SD [(C) to (F)], and individual data points, respectively. ***P < 0.001, ****P < 0.0001. ns, not signficant.

its endogenous ligand VEGF-A$_{164}$ (Fig. 2B and fig. S3D) (*12*). The key residues responsible for contacting the C-terminal R685 of the CendR peptide —Y297, W301, T316, D320, S346, T349 and Y353—are almost identical between the two structures (Fig. 2B and fig. S3D). The R682 and R685 side chains together engage NRP1 via stacked cation-π interactions with NRP1 side chains of Y297 and Y353. By projecting these findings onto the structure of the NRP1 ectodomain, the b1 CendR binding pocket appears to be freely accessible to the S1 CendR peptide (fig. S3E) (*13*).

Site-directed mutagenesis of the S1 R685 residue to aspartic acid drastically reduced GFP-S1$^{493\text{-}685}$ immunoprecipitation by mCherry-b1, confirming the critical role of the C-terminal arginine (Fig. 2C). Mutagenesis of the T316 residue within the mCherry-b1 domain of NRP1 to arginine also reduced association with GFP-S1$^{493\text{-}685}$, consistent with its inhibitory impact on VEGF-A$_{164}$ binding (*12*) (Fig. 2D). Accordingly, incubation of mCherry-b1 with VSV particles pseudotyped with trimeric S resulted in immunoprecipitation of processed forms of S1, which was dependent on the T316 residue (fig. S3F). Next, we transiently expressed either GFP, full-length NRP1 wt-GFP, or full length NRP1-GFP harboring the T316R mutation in HeLa^{NRP1KO}+ACE2 cells. GFP expression and ACE2 expression levels were comparable and both constructs retained similar cell surface localization (fig. S3, G and H). SARS-CoV-2 infection was significantly enhanced in cells expressing NRP1 wt-GFP compared to GFP control, whereas it was not enhanced in cells expressing the T316R mutant (Fig. 2E). Thus, the SARS-CoV-2 S1 CendR and NRP1 interaction promotes infection.

To establish the functional relevance of the S1 CendR-NRP1 interaction, we screened monoclonal antibodies (mAb#1, mAb#2, mAb#3) raised against the NRP1 b1b2 ectodomain. All three bound to the NRP1 b1b2 domain, displayed staining by immunofluorescence

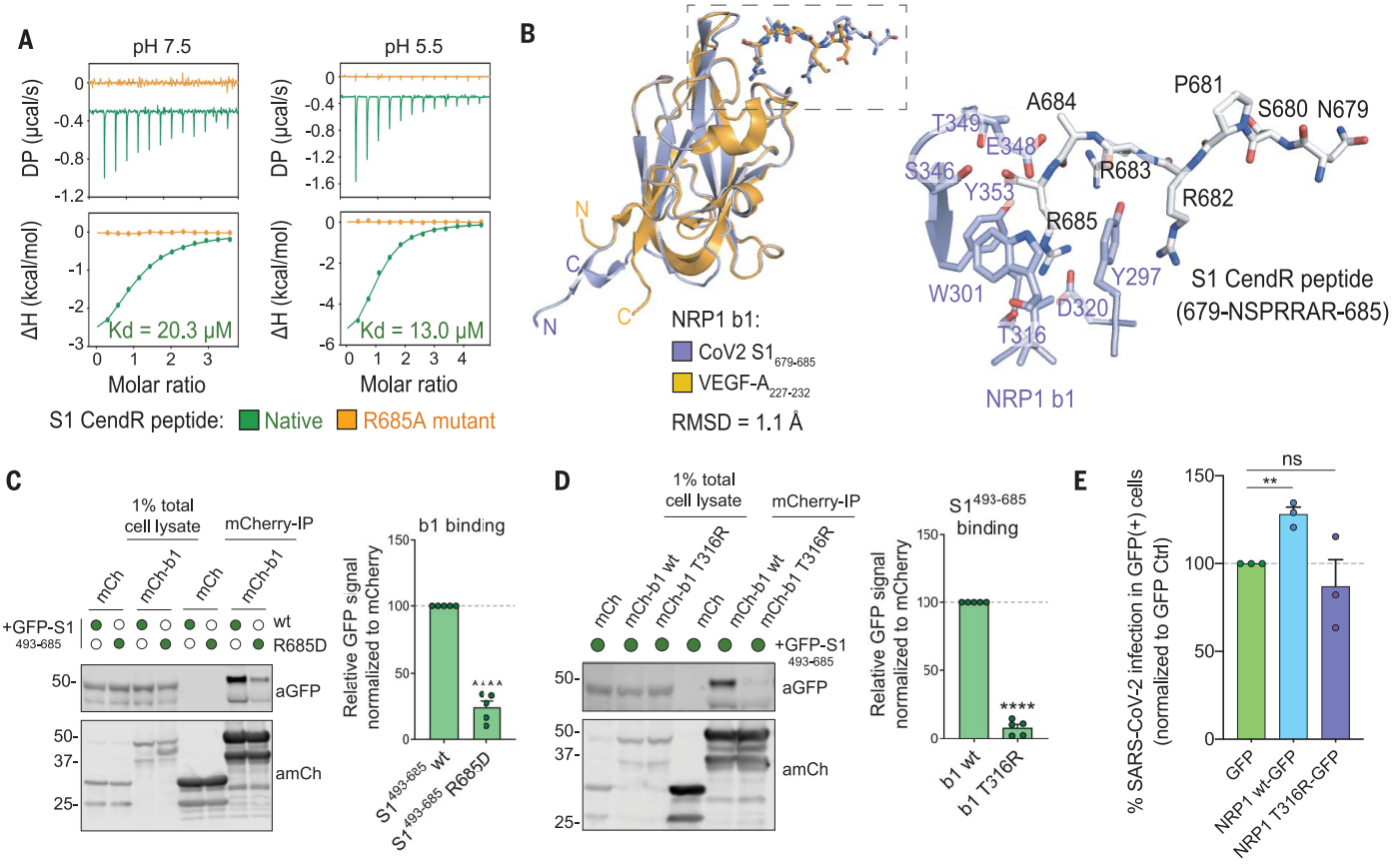

Fig. 2. Molecular basis for CendR binding of SARS-CoV-2 S1 with NRP1. (**A**) Binding of NRP1 b1 with native (green line) and mutant (orange line) form of S1 CendR peptide (corresponding to residues 679 to 685) by ITC at two different pH conditions (N = 3 independent experiments). All ITC graphs represents the integrated and normalized data fit with 1-to-1 ratio binding. (**B**) (Left) NRP1 b1–S1 CendR peptide complex superposed with NRP1 b1–VEGF-A fusion complex (PDB ID: 4DEQ). Bound peptides are shown in stick representation. RMSD, root mean square deviation. (Right) Enlarged view highlighting the binding of S1 CendR peptide b1. Key binding residues on b1 are shown in stick representation. Abbreviations for the amino acid residues are as follows: A, Ala; D, Asp; E, Glu; N, Asn; P, Pro; R, Arg; S, Ser; T, Thr; W, Trp; and Y, Tyr. (**C**). HEK293T cells were cotransfected with combinations of GFP-tagged $S1^{493-685}$ and $S1^{493-685}$ R685D, and mCherry or mCherry-NRP1 b1, and subjected to mCherry-nanotrap (N = 5 independent experiments). Two-tailed unpaired t test; $P < 0.0001$. (**D**). HEK293T cells were cotransfected with combinations of GFP-tagged $S1^{493-685}$ and mCherry, mCherry-NRP1 b1 or mCherry-NRP1 b1 T316R mutant, and subjected to mCherry-nanotrap (N = 5 independent experiments). Two-tailed unpaired t test; $P < 0.0001$. (**E**) $HeLa^{NRP1KO}$ + ACE2 cells transfected with GFP, NRP1 wt-GFP, or NRP1 T316R-GFP constructs were infected 24 hours later with SARS-CoV-2. At 16 hpi, the cells were fixed and stained for SARS-CoV-2-N, and viral infection was quantified in the GFP-positive subpopulation of cells (N = 3 independent experiments). The percentage of infection was normalized to that of GFP-transfected cells. Two-tailed unpaired t test; $P = 0.002$. The bars, error bars, and circles represent the mean, SEM [(C) and (D)] and SD (E), and individual data points, respectively. $^{**}P < 0.01$, $^{****}P < 0.0001$. ns, not signficant.

in NRP1-expressing PPC-1 (human primary prostate cancer) cells but not in M21 (human melanoma) cells that do not express NRP1 (fig. S4A) (*8*), and stained the extracellular domain of NRP1-GFP expressed in cells (fig. S4B). Of these antibodies, mAb#3, and to a lesser extent mAb#1, bound to the CendR-binding pocket with high specificity, as defined by reduced ability to bind to a b1b2 mutant that targets residues (S346, E348, T349) at the opening of the binding pocket (Fig. 3A) (*12*). Incubation of Caco-2 cells with mAbs#1 and 3 reduced SARS-CoV-2 infection compared to a control mAb targeting avian influenza A virus (H11N3) hemagglutinin (Fig. 3B). Consistent with this, mAb#3 inhibited binding of GFP-$S1^{493-685}$ and mCherry-b1 (Fig. 3C). As a comparison, Caco-2 and Calu-3 cells were incubated with soluble ACE2, which inhibited SARS-CoV-2 infection in both cases (fig. S4C).

Next, we turned to the small molecule EG00229, a selective NRP1 antagonist that binds the b1 CendR binding pocket and inhibits VEGF-A binding (Fig. 3D) (*14*). ITC established that EG00229 bound to the NRP1 b1 domain with a dissociation constant (K_d) of 5.1 and 11.0 µM at pH 7.5 and 5.5, respectively (Fig. 3E). EG00229 inhibited the direct binding between b1 and the S1 CendR peptide, and the immunoprecipitation of GFP-$S1^{493-685}$ by mCherry-b1 (Fig. 3E and fig. S4D). Finally, incubation of Caco-2 cells with EG00229 reduced the efficiency of SARS-CoV-2 infection at 7 and 16 hpi (Fig. 3F). Thus, the SARS-CoV-2 interaction with NRP1 can be targeted to reduce viral infectivity in relevant human cell lines (fig. S5).

Cell entry of SARS-CoV-2 depends on priming by host cell proteases (*5*, *6*, *15*). Our data indicate that a component of SARS-CoV-2 S protein binding to cell surface neuropilins occurs via the S1 CendR motif generated by the furin cleavage of S1/S2. Though not affecting cell surface attachment, this interaction promotes entry and infection by SARS-CoV-2 in physiologically relevant cell lines widely used in the study of COVID-19. The molecular basis for the effect is unclear, but neuropilins are known to mediate the internalization of CendR ligands through an endocytic process resembling macropinocytosis,

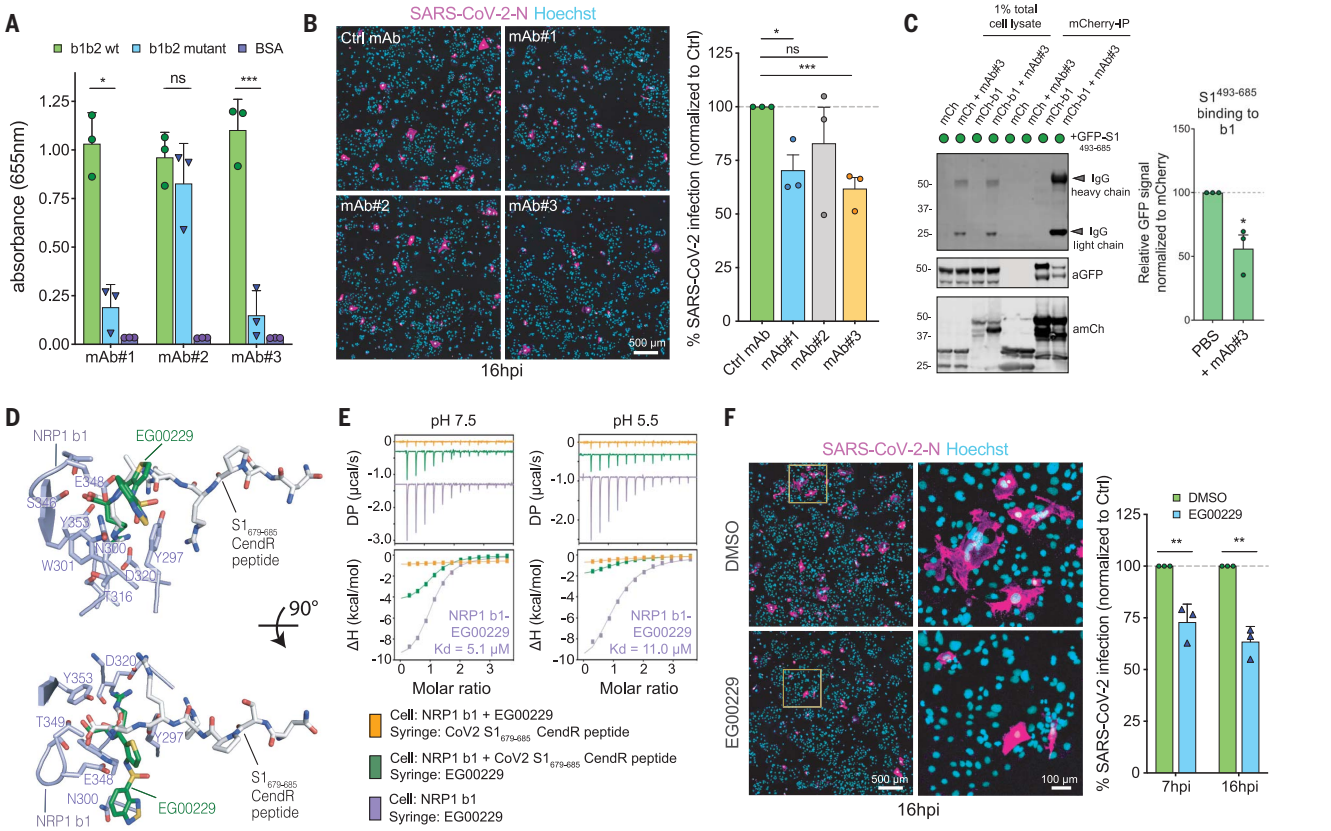

Fig. 3. Selective inhibition of the S1-NRP1 interaction reduces SARS-CoV-2 infection. (**A**) Enzyme-linked immunosorbent assay of anti-NRP1 monoclonal antibodies (mAb#1, mAb#2, mAb#3) at 3 µg/ml using plates coated with NRP1 b1b2 wild type, b1b2 mutant (S346A, E348A, T349A), or bovine serum albumin (BSA), used as a control (N = 3 independent experiments). Binding is represented as arbitrary units of absorbance at 655 nm. Two-tailed unpaired t test; P = 0.0207, 0.2430, 0.0007. (**B**) Cells were first treated with anti-H11N3 (100 µg/ml) (Ctrl) mAb, mAb#1, mAb#2, or mAb#3 for 1 hour before infection with SARS-CoV-2. Cells were fixed at 16 hpi and stained for N protein (magenta) and Hoechst (cyan) (N = 3 independent experiments). Two-tailed unpaired t test; P = 0.015, 0.36, 0.0003. Scale bar, 500 µm. (**C**) HEK293T cells were cotransfected with combinations of mCherry or mCherry-b1 and GFP-tagged S1$^{493-685}$ and subjected to mCherry-nanotrap with or without coincubation with mAb#3 (N = 3 independent experiments). Two-tailed unpaired t test; P = 0.0143. (**D**) NRP1 b1–S1 CendR peptide complex superimposed with NRP1 b1–EG00229 inhibitor complex (PDB ID:3I97). Key binding residues on b1, bound peptides, and EG00229 are shown in stick representation. (**E**) ITC analysis of EG00229 binding to b1 domain of NRP1 at two different pH conditions. Preincubation with EG00229 blocks S1 CendR peptide binding (orange line), and the CendR peptide can reduce binding of EG00229 (green line) (N = 3 independent experiments). All ITC graphs represent the integrated and normalized data fit with 1-to-1 ratio binding. (**F**). Cells were first treated with 100 µM EG00229 or dimethyl sulfoxide before infection with SARS-CoV-2. Cells were fixed at 7 and 16 hpi and stained for N protein (magenta) and Hoechst (cyan) (N = 3 independent experiments). The square regions were enlarged. Scale bars, 500 µm and 100 µm (magnified panels). Two-tailed unpaired t test; P = 0.0059 and 0.0013. The bars, error bars, and circles and triangles represent the mean, SEM (C) and SD [(A), (B), and (F)], and individual data points, respectively. *P < 0.05, **P < 0.01, ***P < 0.001.

(*8*, *16*, *17*). Notably, gene expression analysis has revealed an up-regulation of NRP1 and NRP2 in lung tissue from COVID-19 patients (*18*). A SARS-CoV-2 virus with a natural deletion of the S1/S2 furin cleavage site demonstrated attenuated pathogenicity in hamster models (*19*). NRP1 binding to the CendR peptide in S1 is thus likely to play a role in the increased infectivity of SARS-CoV-2 compared with SARS-CoV. The ability to target this specific interaction may provide a route for COVID-19 therapies.

REFERENCES AND NOTES

1. WHO Coronavirus disease, 2019 (COVID-19) Weekly Epidemiological Update – 31 August 2020. https://www.who.int/docs/default-source/coronaviruse/situation-reports/20200831-weekly-epi-update-3.pdf?sfvrsn=d7032a2a_4
2. E. Dong, H. Du, L. Gardner, *Lancet Infect. Dis.* **20**, 533–534 (2020).
3. D. Wrapp *et al.*, *Science* **367**, 1260–1263 (2020).
4. A. C. Walls *et al.*, *Cell* **181**, 281–292.e6 (2020).
5. M. Hoffmann, H. Kleine-Weber, S. Pöhlmann, *Mol. Cell* **78**, 779–784.e5 (2020).
6. M. Hoffmann *et al.*, *Cell* **181**, 271–280.e8 (2020).
7. J. Shang *et al.*, *Proc. Natl. Acad. Sci. U.S.A.* **117**, 11727–11734 (2020).
8. T. Teesalu, K. N. Sugahara, V. R. Kotamraju, E. Ruoslahti, *Proc. Natl. Acad. Sci. U.S.A.* **106**, 16157–16162 (2009).
9. H. F. Guo, C. W. Vander Kooi, *J. Biol. Chem.* **290**, 29120–29126 (2015).
10. A. Plein, A. Fantin, C. Ruhrberg, *Microcirculation* **21**, 315–323 (2014).
11. R. Hollandi *et al.*, *Cell Syst.* **10**, 453–458.e6 (2020).
12. M. W. Parker, P. Xu, X. Li, C. W. Vander Kooi, *J. Biol. Chem.* **287**, 11082–11089 (2012).
13. B. J. Janssen *et al.*, *Nat. Struct. Mol. Biol.* **19**, 1293–1299 (2012).
14. A. Jarvis *et al.*, *J. Med. Chem.* **53**, 2215–2226 (2010).
15. J. K. Millet, G. R. Whittaker, *Virology* **517**, 3–8 (2018).
16. M. Simons, E. Gordon, L. Claesson-Welsh, *Nat. Rev. Mol. Cell Biol.* **17**, 611–625 (2016).
17. H. B. Pang *et al.*, *Nat. Commun.* **5**, 4904 (2014).
18. M. Ackermann *et al.*, *N. Engl. J. Med.* **383**, 120–128 (2020).
19. S.-Y. Lau *et al.*, *Emerg. Microbes Infect.* **9**, 837–842 (2020).

ACKNOWLEDGMENTS

We thank the Bristol Synthetic Biology Centre and the Advanced Computing Research Centre for provision of HPC (Bluegem), and the University of Bristol Wolfson Bioimaging Facility. We thank the University of Queensland Remote Operation Crystallisation and X-ray facility (UQ-ROCX) and the staff for their support with the crystallization experiments, and the staff of the Australian Synchrotron for assistance with x-ray diffraction data collection.

Funding: J.L.D. was supported by a Wellcome Trust studentship from the Dynamic Molecular Cell Biology Ph.D. program (203959/Z/16/Z), C.A.P. was supported by Beca Fundación Ramón Areces Estudios Postdoctorales en el Extranjero, and M.K.W. was supported by an MRC grant (MR/R020566/1) awarded to A.D.D. This project has received funding from the MRC (MR/P018807/1), Wellcome Trust (104568/Z/14/2), Lister Institute of Preventive Medicine, and Elizabeth Blackwell Institute for Health Research Rapid Response Call (COVID-19) awarded to P.J.C, the European Research Council under the European Union's Horizon 2020

research and innovation program (No 856581 - CHUbVi), and from MRC-AMED (MR/T028769/1) awarded to Y.Y., the Swiss National Science Foundation and Kanton Zurich awarded to U.F.G. B.M.C. is supported by an Australian National Health and Medical Research Council (NHMRC) Senior Research Fellowship (APP1136021) and Project Grant (APP1156493), and the United States Food and Drug Administration grant no. HHSF223201510104C "Ebola Virus Disease: correlates of protection, determinants of outcome and clinical management" amended to incorporate urgent COVID-19 studies awarded to J.A.H., A.D.D., and D.A.M. R.H. and P.H. acknowledge support from the LENDULET-BIOMAG Grant (2018-342), from H2020-discovAIR (874656), and from Chan Zuckerberg Initiative, Seed Networks for the HCA-DVP. T.T. was supported by the European Regional Development Fund (Project no. 2014-2020.4.01.15-0012), by European Research Council grant GLIOGUIDE and Estonian Research Council (grants PRG230 and EAG79, to T.T.). **Author contributions:** J.L.D., B.S., A.H., P.J.C., and Y.Y. conceived the study. J.L.D., B.S., K.K, and Y.Y. performed most of the experiments. K.K., M.K.W., D.A.M., and A.D.D. performed all work with infectious SARS-CoV-2 supervised by A.D.D. M.K.W. and A.D.D. isolated SARS-CoV-2 strains used for the work. K.C., C.A.P., M.B., L.S.G., U.F.G., K.K., R.B.S., D.K.S., J.A.H., and T.T. did experimental work and/or provided essential reagents. R.H. and P.H. performed image analysis. B.S., A.D.D., B.M.C., P.J.C., and Y.Y. supervised the research. J.L.D., B.S., A.D.D., P.J.C., and Y.Y. wrote the manuscript and made the figures. All authors read and approved the final manuscript. **Competing interests:** T.T. is an inventor of patents on CendR peptides and a shareholder of Cend Therapeutics Inc., a company that holds a license for the CendR peptides and is developing the peptides for cancer therapy. J.A.H. is a member of the Department of Health, New and Emerging Respiratory Virus Threats Advisory Group (NERVTAG) and the Department of Health, Testing Advisory Group. U.F.G. is a consultant to F. Hoffmann–La Roche Ltd, Switzerland. All other authors declare no competing interests. **Data and materials availability:** Coordinates and structure factors for the NRP1 b1-S1 CendR peptide complex have been deposited at the Protein Data Bank (PDB) with accession code 7JJC. All other data are available in the manuscript or the supplementary materials.

SUPPLEMENTARY MATERIALS

science.sciencemag.org/content/370/6518/861/suppl/DC1
Materials and Methods
Figs. S1 to S5
Tables S1 to S3
References (*20*–*33*)
MDAR Reproducibility Checklist

View/request a protocol for this paper from *Bio-protocol*.

14 June 2020; accepted 12 October 2020
Published online 20 October 2020
10.1126/science.abd3072

Science

Neuropilin-1 is a host factor for SARS-CoV-2 infection

James L. Daly, Boris Simonetti, Katja Klein, Kai-En Chen, Maia Kavanagh Williamson, Carlos Antón-Plágaro, Deborah K. Shoemark, Lorena Simón-Gracia, Michael Bauer, Reka Hollandi, Urs F. Greber, Peter Horvath, Richard B. Sessions, Ari Helenius, Julian A. Hiscox, Tambet Teesalu, David A. Matthews, Andrew D. Davidson, Brett M. Collins, Peter J. Cullen and Yohei Yamauchi

Science **370** (6518), 861-865.
DOI: 10.1126/science.abd3072originally published online October 20, 2020

Another host factor for SARS-CoV-2

Virus-host interactions determine cellular entry and spreading in tissues. Severe acute respiratory syndrome coronavirus 2 (SARS-CoV-2) and the earlier SARS-CoV use angiotensin-converting enzyme 2 (ACE2) as a receptor; however, their tissue tropism differs, raising the possibility that additional host factors are involved. The spike protein of SARS-CoV-2 contains a cleavage site for the protease furin that is absent from SARS-CoV (see the Perspective by Kielian). Cantuti-Castelvetri *et al.* now show that neuropilin-1 (NRP1), which is known to bind furin-cleaved substrates, potentiates SARS-CoV-2 infectivity. NRP1 is abundantly expressed in the respiratory and olfactory epithelium, with highest expression in endothelial and epithelial cells. Daly *et al.* found that the furin-cleaved S1 fragment of the spike protein binds directly to cell surface NRP1 and blocking this interaction with a small-molecule inhibitor or monoclonal antibodies reduced viral infection in cell culture. Understanding the role of NRP1 in SARS-CoV-2 infection may suggest potential targets for future antiviral therapeutics.

Science, this issue p. 856, p. 861; see also p. 765

Science (print ISSN 0036-8075; online ISSN 1095-9203) is published by the American Association for the Advancement of Science, 1200 New York Avenue NW, Washington, DC 20005. The title *Science* is a registered trademark of AAAS.